DINAME 2023 - Proceedings of the XIX International Symposium on Dynamic Problems of Mechanics,
A.S. De Paula, A.T. Fabro and M.R. Machado (Editors), ABCM.
Pirenópolis, Go, Brazil, February 26th to March 3rd, 2023

Experimental Insights on the Dynamics of Submerged Flexible Pipes Discharging Water in Post-Critical Regime

Wagner A. Defensor Filho[1], Celso P. Pesce [1], Guilherme J. Vernizzi[1], Vitor Schwenck F. M.[1]

[1] Offshore Mechanics Laboratory, Escola Politécnica, University of São Paulo, Av. Professor Lúcio Martins Rodrigues, Tv. 4, n. 434, São Paulo – SP, 05508-020, Brazil

Abstract: This work brings experimental results of an innovative test campaign with submerged hanging cantilevered flexible pipes under discharging flow excitation in post-critical dynamic regime. The thresholds of instability were identified with root-loci diagrams. An underwater non-invasive optical tracking system was used to directly acquire the Cartesian displacements of predefined points of the pipes. Highly nonlinear dynamic behaviors were revealed in the form of flutter instabilities. Moreover, internal resonances with 1:1 and 2:1 frequency ratio were identified, the latter one recognized as dual-resonance regime.

Keywords: Pipes Conveying Fluid, Discharging flow, Post-Critical Regime, Flutter Instability, Dual-Resonance

INTRODUCTION

The search for predicting the behavior of flexible pipes under the excitation of internal flow is a quest that has been enduring for more than half a century. As a matter of fact, the first study recognized as an attempt to formulate the dynamics of pipes conveying fluid is due to François Bourrières in 1939. That work was 'lost' on the shedding of the Second World War. In the '50s and '60s, all the derivation had already been done again by other authors, mainly motivated by technological demands of the time. It was only in the '70s that Bourrières' work was rediscovered (Païdoussis, 2022).

Several works tackled such subjected over the years. In particular, the problem of a cantilever pipe ejecting fluid is known as the Benjamin's problem due to its well-known study of a system of rigid and articulated pipes ejecting fluid (Benjamin, 1961), which stated the basis of understanding for this specific configuration, identifying through the stability analysis of the state of equilibrium, the existence of self-excited oscillations instability when the internal flow surpasses a specific velocity value. More recently, Païdoussis (2014) presented a treatise in this book by discussing the dynamics of slender structures subjected to internal and/or external axial flows in different configurations and boundary conditions. In Païdoussis (2022), a comprehensive overview on the topic of pipes conveying fluid is discussed, in an attempt of creating a conductor thread over the numerous publications on the theme. The list of interesting publications is long, with the present text referring to only a few of the most prominent.

A certain variety of configurations belongs to this type of problem such as articulated (discrete) and continuous flexible pipes; in the presence or not of gravity effects (i.e. vertical, either hanging or standing, or horizontal configurations); with clamped-free, clamped-pinned or pinned-pinned boundary conditions; aspirating or discharging fluid. As stated in Païdoussis and Li (1993), the problem regarding the dynamics of pipes conveying fluid became a 'generic paradigm due its kaleidoscope of interesting dynamical behavior'.

The present study focus on the dynamics of immersed hanging cantilevered flexible pipes discharging water in post-critical regime. The motivation comes from the fact that this is a rather simple configuration and yet displays a fine example of highly complex and nonlinear dynamic behavior. It is already stablished in the literature that this system (hanging cantilever) presents a threshold of instability related to a specific value of internal flow velocity, identified as critical value. Below such critical value, the internal flow implies in positive damping in the system, whereas above such value, damping becomes negative and the system presents steady high amplitude flutter instability. Mathematically, the flutter instability is a Hopf bifurcation of a specific natural mode of vibration of the system, where the associated eigenvalue presents positive real part and non-zero imaginary part. The critical flow velocity value represents therefore the threshold between stable and unstable regimes.

To contribute to the study of such problem, an innovative experimental campaign was conducted at the "Instituto de Pesquisas Tecnológicas do Estado de São Paulo" – IPT towing tank facility, aiming at simultaneously assessing the dynamics of submerged cantilevered flexible pipes, under pure internal water flow excitation, in post-critical regime, using non-invasive instrumentation, thus having no precedents in the respective technical literature. The results henceforward presented are meant to be used as benchmark data for simulations of mathematical models that tackle problems involving submerged hanging cantilever flexible pipes conveying fluid in discharging condition.

Experimental Campaign at IPT

Three experimental models composed of a flexible rubber hose and a rigid ballast attached at the free end were designed and constructed with the support of an implementation of the mathematical model presented in Orsino *et al.* (2022), to be tested in the scenarios of pure and combined excitation cases of towing, harmonic motion applied to the top and internal flow on aspirating and discharging conditions. The new database is quite rich. The present text addresses the case of pure discharging flow for its very interesting results regarding high amplitude nonlinear dynamics.

Since the models are based on a ballasted-hose concept, they were named according to the acronym 'BH' followed by the number of the natural mode of vibration (n = 1, 2, 3) designed to be the dominant one under towing excitation: BH-1, BH-2 and BH-3 (see Fig. 1). Henceforward, the subscripts 'H' and 'B' refer to hose and ballast, respectively.

The towing tank at IPT is 240 m long, 6 m wide and 3.5 m deep, with maximum towing carriage speed of 4.5 m/s. The models are composed of a flexible nitrile rubber hose with fiber reinforcement, presenting linear density μ_H = 0.56 kg/m, axial stiffness $EA_H = 12.5\times10^3$ N and bending stiffness EI_H = 1.23 Nm², coupled to a brass ballast with corresponding values μ_B = 4.15 kg/m, EA_B = 49.9 10^6 N and EI_B = 4.91 10^3 Nm². Both the hose and ballast present the same internal and external diameters of $Ø_I$ = 22 mm and $Ø_E$ = 33 mm, respectively. Model BH-2 total length is L_M = 1.705 m with second natural mode frequency of f_{2y} = 1.18 Hz. Model BH-3 length is L_M = 3.030 m and its third natural mode frequency is f_{3y} = 1.15 Hz. Table 1 presents some of the main parameters used in the design. Table 2 shows the measured natural frequencies in water. The differences between the values in the x and y directions are due to the presence of a residual curvature in the hose, located in the xz plane and oriented to negative x direction, result of its manufacturing and cooling process.

Root-loci diagrams (Fig. 2) obtained from the linearized form of the mentioned mathematical model present the natural periods of the experimental models in water as function of the internal flow velocity in discharging condition. As aforementioned, the value in which a natural mode shifts from stable to unstable regime was identified as a threshold of instability and labeled as the internal critical flow velocity, V_C. The *root-loci* for model BH-2 (Fig. 2, on the left) presents the beginning of instability at 6.80 m/s for the second natural mode of vibration, while, for model BH-3 (Fig. 2, on the right), the instability first happens for the third natural mode at 6.66 m/s. Values of 0.5 V_C and 1.0 V_C were tested with the present text bringing only the latter case for models BH-2 and BH-3, since the corresponding value was never reached for model BH-1. The structural displacements were directly acquired with the optical Qualisys Tracking Manager™ (QTM) system, which tracks the 3D Cartesian coordinates of reflective tapes placed along the length of the models. For another example of the use of the QTM system and an innovative experimental data analysis of flexible cylinders under VIV, the reader is oriented to Defensor Filho *et al.* (2022).

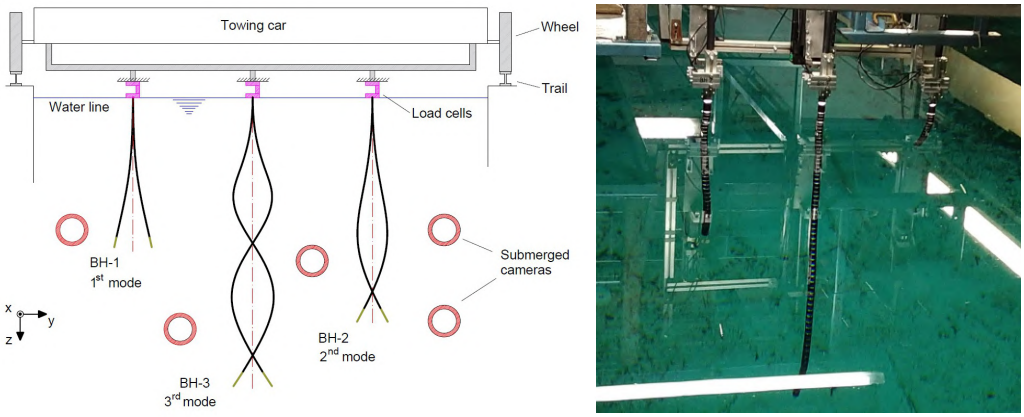

Figure 1: (Left) Sketch of the three flexible models arrangement exhibiting oscillations in the 1st, 3rd and 2nd natural modes of vibration (from left to right) of the vertical cantilever beam configuration. (Right) Experimental models in their actual assembly in the towing tank (from left to right: BH-2, BH-3 and BH-1).

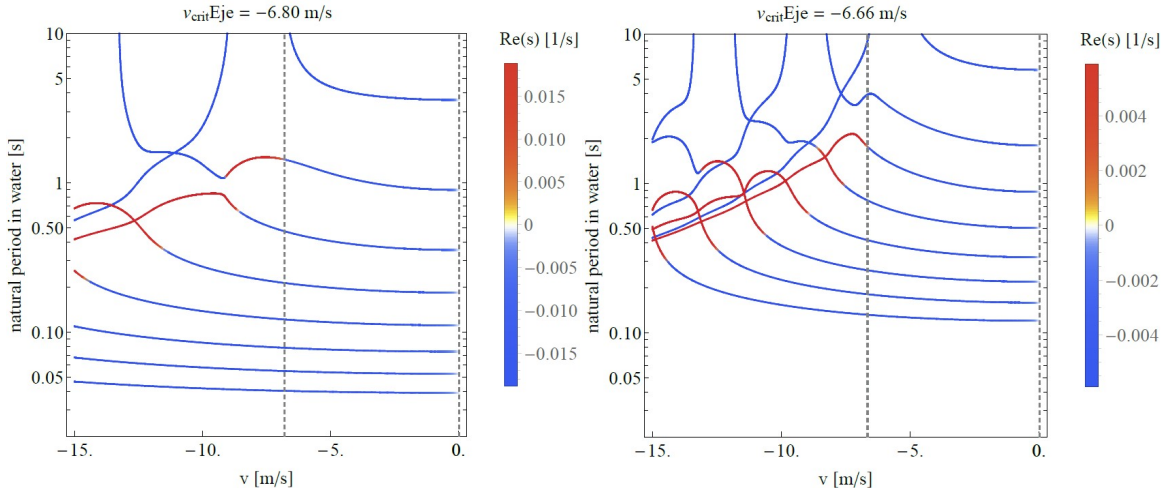

Figure 2: *Root-loci* diagrams. (Left) Model BH-2; (right) model BH-3. Cold colors indicate stability and warm colors indicate instability. Natural modes of vibration ordered from top to bottom in the reference configuration (v=0). Dashed lines indicate the critical velocity. Negative values of the horizontal axis indicate discharging flow.

Table 1: Experimental models parameters.

	Parameter	Experimental model	
		BH-2	BH-3
Hose – Nitrile rubber	Linear density - μ_H [kg/m]	0.56	0.56
	Axial stiffness - EA_H [N]	$12.5\ 10^3$	$12.5\ 10^3$
	Bending stiffness - EI_H [Nm^2]	1.23	1.23
	Length - L_H [m]	1.595	2.857
	Mass - m_H [kg]	0.89	1.60
Ballast - Brass	Linear density - μ_B [kg/m]	4.15	4.15
	Axial stiffness - EA_B [N]	$49.9\ 10^6$	$49.9\ 10^6$
	Bending stiffness – EI_B [Nm^2]	$4.91\ 10^3$	$4.91\ 10^3$
	Length - L_B [m]	0.110	0.173
	Mass - m_B [kg]	0.46	0.72
Complete model	VIV dominant crosswise natural mode - n	2nd	3rd
	Frequency of mode n in water – f_{ny} [Hz]	1.18	1.15
	External diameter - $Ø_E$ [mm]	33	33
	Internal diameter - $Ø_I$ [mm]	22	22
	Length ratio - L_B/L_H [%]	6.90	6.06
	Total length - L_M [m]	1.705	3.030
	Slenderness – $L_M/Ø_E$	51.67	91.82
	Mass - m_M [kg]	1.35	2.32
	Mass of internal water - m_{iw} [kg]	0.65	1.15
	Mass of displaced water - m_{dw} [kg]	1.46	2.59
	Mass ratio – m^*	1.37	1.34
	Discharging – Modes bifurcating	2	3
	Discharging critical velocity – V_C [m/s]	6.80	6.66

Table 2: Measured natural frequencies in water.

Experimental model	Direction	Natural Frequency [Hz] – Mode n		
		1	2	3
BH-2	x	0.29	1.15	
	y	0.27	1.18	
BH-3	x	0.18	0.56	1.17
	y	0.17	0.56	1.15

RESULTS

This section presents the results concerning the experimental models BH-2 and BH-3 in pure discharging flow at 1 V_C in post-critical condition. The discussion addresses the displacements of the models with the respective trajectories and amplitude spectra.

Figures 3(a), (b) and (c) present the orbits projection for model BH-2 onto the *xz*, *yz* and *xy* (horizontal) planes, respectively, in six different arc length positions, $S = z_0/L = 0.00, 0.18, 0.41, 0.65, 0.88$ and 1.00, with z_0 being the corresponding initial vertical position and L the total length of the model. $S = 0.00$ and 1.00 refer to the clamp and the free tip, respectively. The tip presents displacements of large amplitudes reaching $ax^* = ax/L \approx 0.4$ and more than half of the length of the model in the other direction, $ay^* = ay/L > 0.5$. One can notice gaps, specifically in the orbits at $S = 0.65$, which are due to moments were parts of the hose exceed the tracking volume of the underwater cameras. Three-dimensional orbits are showed in Fig. 3(d) along with a vertical black line that illustrates the hose at a specific instant of time, which was obtained with an *ad hoc* pre-processing interpolation algorithm that recreates lost signals. The model rotates in the counter-clockwise direction and presents simple oval-shaped trajectories. The large nonlinear amplitudes are clearly seen in the deformed configuration snapshots, Figs. 3(e) and (f), where warm and cold colors indicate positive and negative coordinates, respectively, with respect to the reference point (the clamp).

Figure 4(a) depicts the displacement time series at the free end and the respective amplitude spectra, in the x and y directions. One may see that the highest peaks appear at 0.28 Hz, practically the exact value of the first natural frequencies, $f_{1x,y}$ (see Tab. 2). This indicates an internal resonance with 1:1 frequency ratio, which is the cause for the oval shape trajectories. Figure 4(b) shows the time series of the force components, measured at the clamp, along with the corresponding amplitude spectra. The signals present energy content at same frequencies as shown by the free end displacements spectra presented in both directions. In every time series, the dashed vertical lines indicate the selected piece of time series used to calculate the amplitude spectrum.

Figure 5(a) shows the amplitude spectra along the length of the model, as function of the normalized frequency $f^*_{x,y} = f_{x,y} / f_{2y}$, in a distribution consistent to the cantilever first natural mode shape, in both directions, and, as mentioned

before, in the same frequency of oscillation. Low energy components of higher modes are present. In Fig. 5(b), amplitude scalograms along the length of the model, as function of the dimensionless time $t^* = t\ f_{2y}$, present oscillations between positive and negative coordinates in a distribution that also resembles the cantilever first mode shape, regardless the direction.

The result panels for model BH-3 are similar. The orbital projections, Figs. 6(a), (b) and (c), refer to eight arc length positions, S = 0.00, 0.13, 0.29, 0.45, 0.61, 0.77, 0.90 and 1.00. The tip presents amplitude displacements of order $ax^* \approx 0.3$ and $ay^* \approx 0.4$, respectively. The crossing points are displaced to negative x coordinates, as can be seen in Fig. 6(c), which is related to the presence of the residual curvature. The 3D orbits, Fig. 6(d), also presents a vertical black line illustrating the hose at a specific instant of time. One can notice that the gaps are more frequent in the displacements at the tip for this model. The deformed configuration snapshots, Figs. 6(e) and (f), depicts a dynamic behavior revealing more complex displacement patterns with well-defined eight-shape trajectories.

In this case, the displacement time series of the free end and the respective amplitude spectra, Fig. 7(a), show different frequencies for the highest peaks, with 0.48 Hz and 0.24 Hz, in the x and y directions, respectively. This indicates a 2:1 internal resonance, also known as dual-resonance regime, which is the cause for the eight-shape trajectories. The force components amplitude spectra, Fig. 7(b), show peaks of response at the same frequencies as those presented by the free end displacements spectra. Once again, the dashed vertical lines indicate the selected analysis window.

The amplitude spectra along the length of the model, as function of the normalized frequency $f^*_{x,y} = f_{x,y} / f_{3y,}$ Fig. 8(a), presents an amplitude distribution consistent to the cantilever first mode (as in the previous model), in both directions, however, in a 2:1 frequency ratio. Again, low energy components of higher modes are visible. The amplitude scalograms along the length of the model, as function of the dimensionless time $t^* = t\ f_{3y}$, Fig. 8(b), also shows the oscillations similar to the cantilever first mode shape.

CONCLUSION

An innovative experimental campaign assessed the dynamic behavior of two submerged hanging cantilevered flexible pipes with a rigid ballast attached at the free end under the dynamic excitation of internal flow in post-critical regime. Large three-dimensional amplitude motions related to flutter instability were identified in both experimental models, depicting highly non-linear oscillations. Internal resonances were revealed in both models, with the shortest one presenting a 1:1 frequency ratio between oscillations in the *x* and *y* directions, and the longest one, presenting a 2:1 internal resonance, also known as dual-resonance regime. Despite the *root-loci* diagrams indicate the second and the third cantilevered natural modes (for models BH-2 and BH-3, respectively) as the ones that would present instability when the respective internal flow critical velocities are surpassed, the analysis revealed that, in steady state regime, the post-critical dynamics appeared to be dominated by first-mode like oscillations.

ACKNOWLEDGMENTS

The authors would like to thank to Shell/2021 SWIR R&D Project FUSP 3456. The first author acknowledges a PPGEN Capes PhD scholarship. The second author acknowledges a CNPq grant nº 308230/2018-3. The third and fourth authors acknowledge FAPESP scholarships nº 2016/25457-1 and nº 2021/04434-1, respectively. The first author is very much grateful to Professor Guilherme R. Franzini (CNPq grant nº 305945/2020-3) for all his support. IPT technical staff is gratefully acknowleged.

REFERENCES

Benjamin, T.B., 1961, “Dynamics Of A System Of Articulated Pipes Conveying Fluid I. Theory”, Proceedings of the Royal Society of London, Series A, Vol. 261.

Defensor Filho, W.A., Franzini, G.R. and Pesce, C.P., 2022, “An experimental investigation on the dual-resonance revealed in the VIV of flexible cantilevers with orthotropic bending stiffness”, Applied Ocean Research, Vol. 126, https://doi.org/10.1016./j.apor.2022.103263.

Orsino, R.M.M., Pesce, C.P., Toni, F.G., Defensor Filho, W.A. and Franzini, G.R., 2022, “A 3D Nonlinear Reduced-Order Model of a Cantilevered Aspirating Pipe Under VIV”, In: Advances in Nonlinear Dynamics. Springer, Cham, pp. 107-117.

Païdoussis, M.P., Li, G.X., 1993. “Pipes Conveying Fluid: A Model Dynamical Problem”, Journal of Fluids and Structures, Vol. 7, pp. 137-204.

Païdoussis, M.P., 2014, “Fluid-Structure Interactions: Slender Structures And Axial Flow”, Vol. 1, second ed. Academic Press, Oxford.

Païdoussis, M.P., 2022, “Pipes Conveying Fluid: A Fertile Dynamics Problem”, Journal of Fluids and Structures, Vol. 114, https://doi.org/10.1016/j.jfluidstructs.2022.103664.

RESPONSIBILITY NOTICE

The authors are the only responsible for the printed material included in this paper.

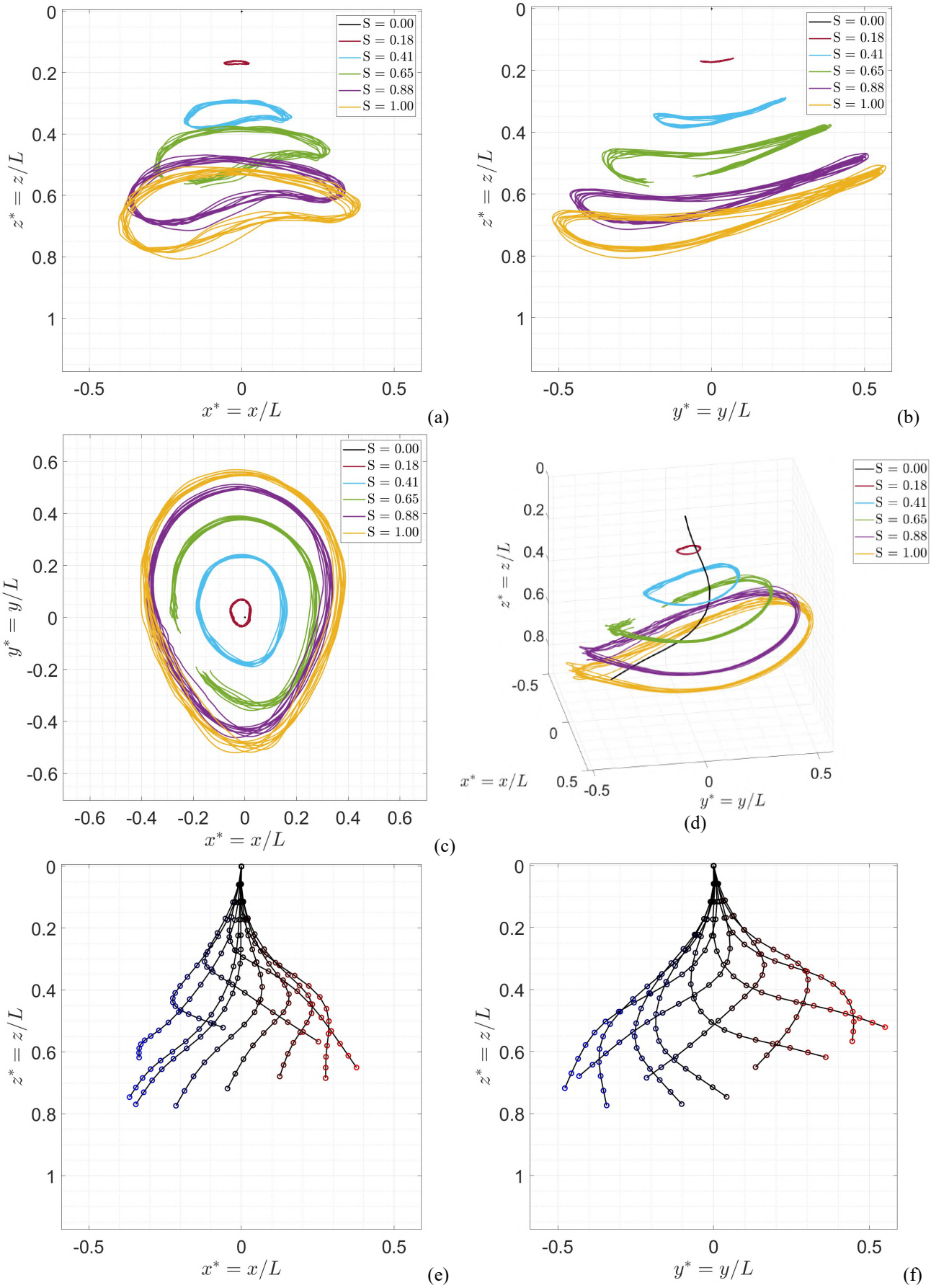

Figure 3: (a), (b) and (c) Orbits projections onto the *xz*, *yz* and *xy* (horizontal) planes, respectively. (d) Three-dimensional orbits. (e) and (f) Deformed configuration snapshots in *x* and *y* directions, respectively, along vertical axis. Warm colors: positive coordinates; cold colors: negative coordinates. Scales 1:1. Model BH-2.

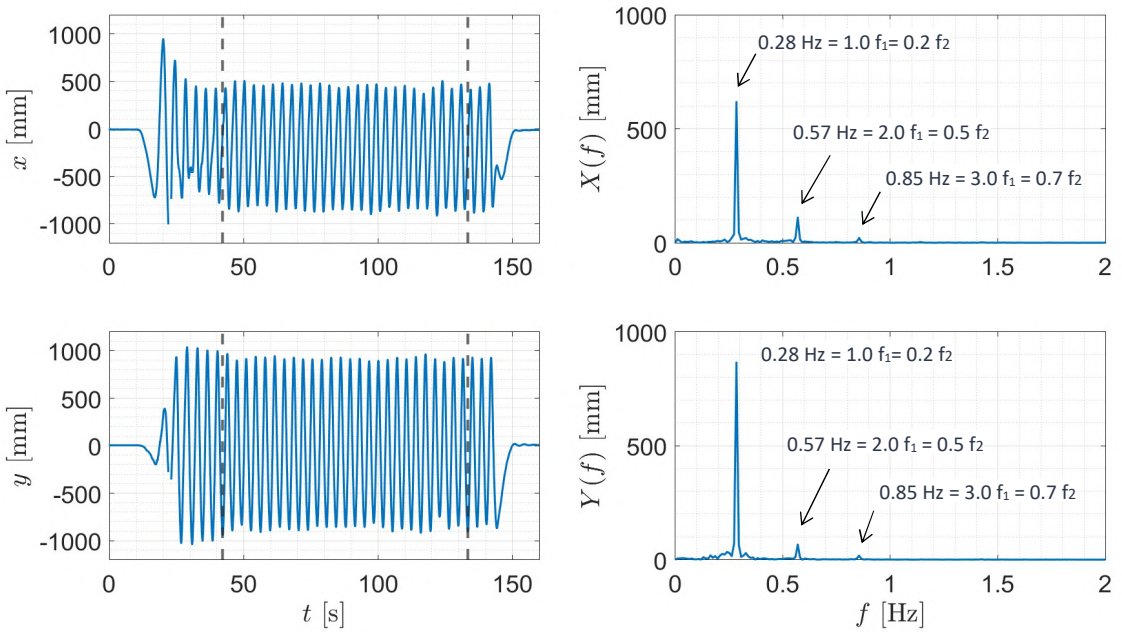

(a)

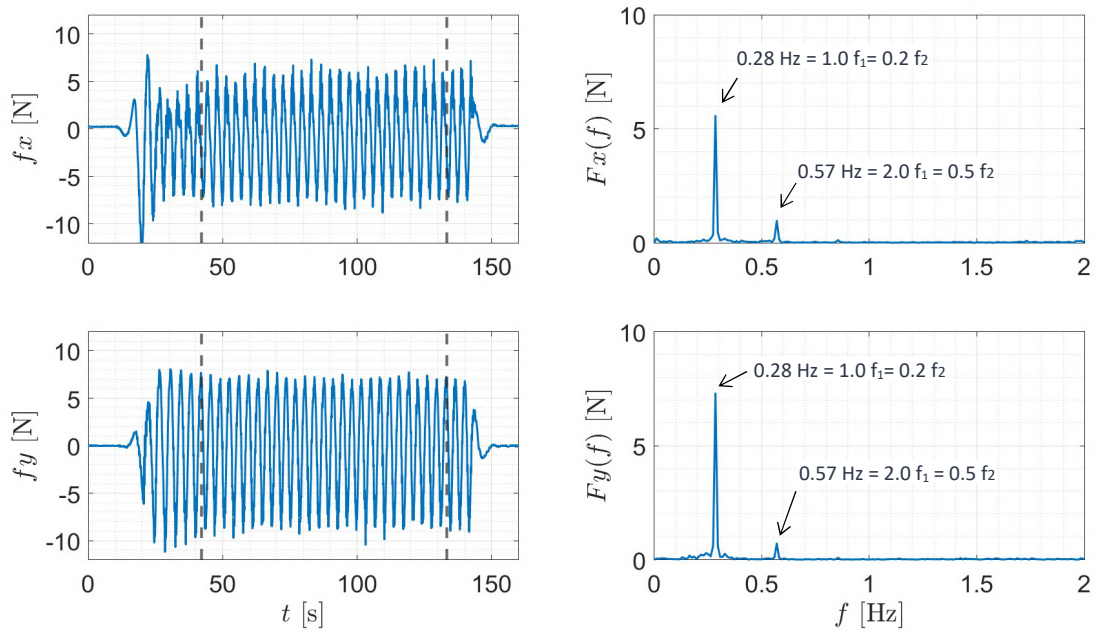

(b)

Figure 4: (a) Tip time series and amplitude spectrum in *x* and *y* directions. (b) Reaction force components at the clamp: time series and amplitude spectrum. Vertical dashed lines indicate the selected part of the signal. Model BH-2.

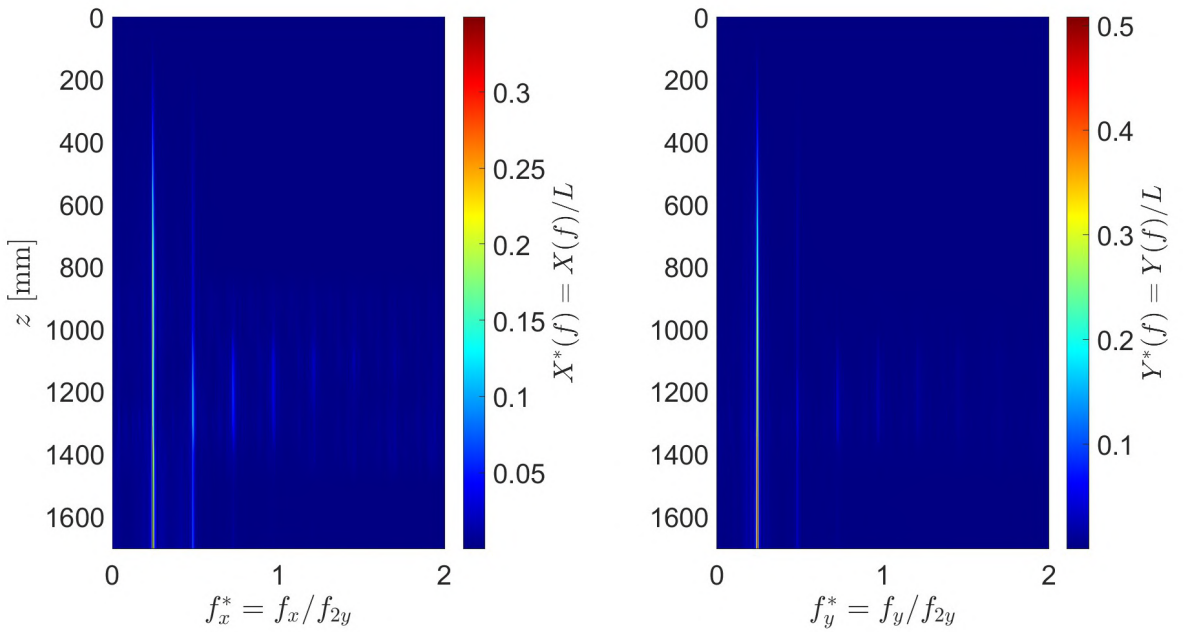

(a)

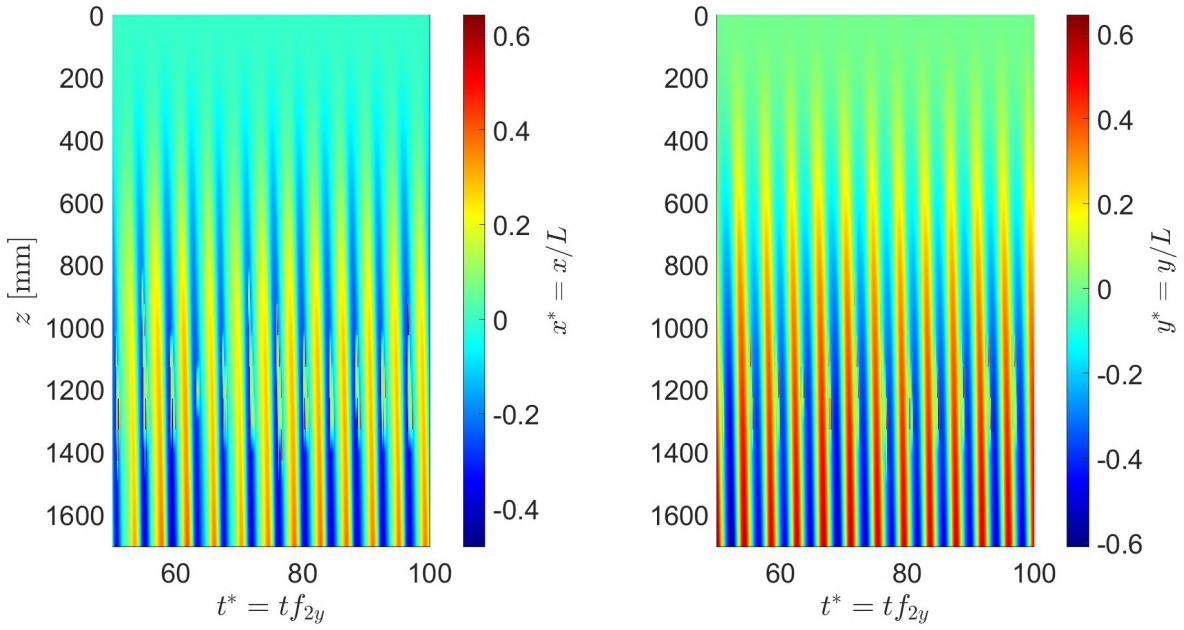

(b)

Figure 5: (a) Amplitude spectra. (b) Amplitude scalograms. Both, along the model's length. *x* (left) and *y* (right) directions. Model BH-2.

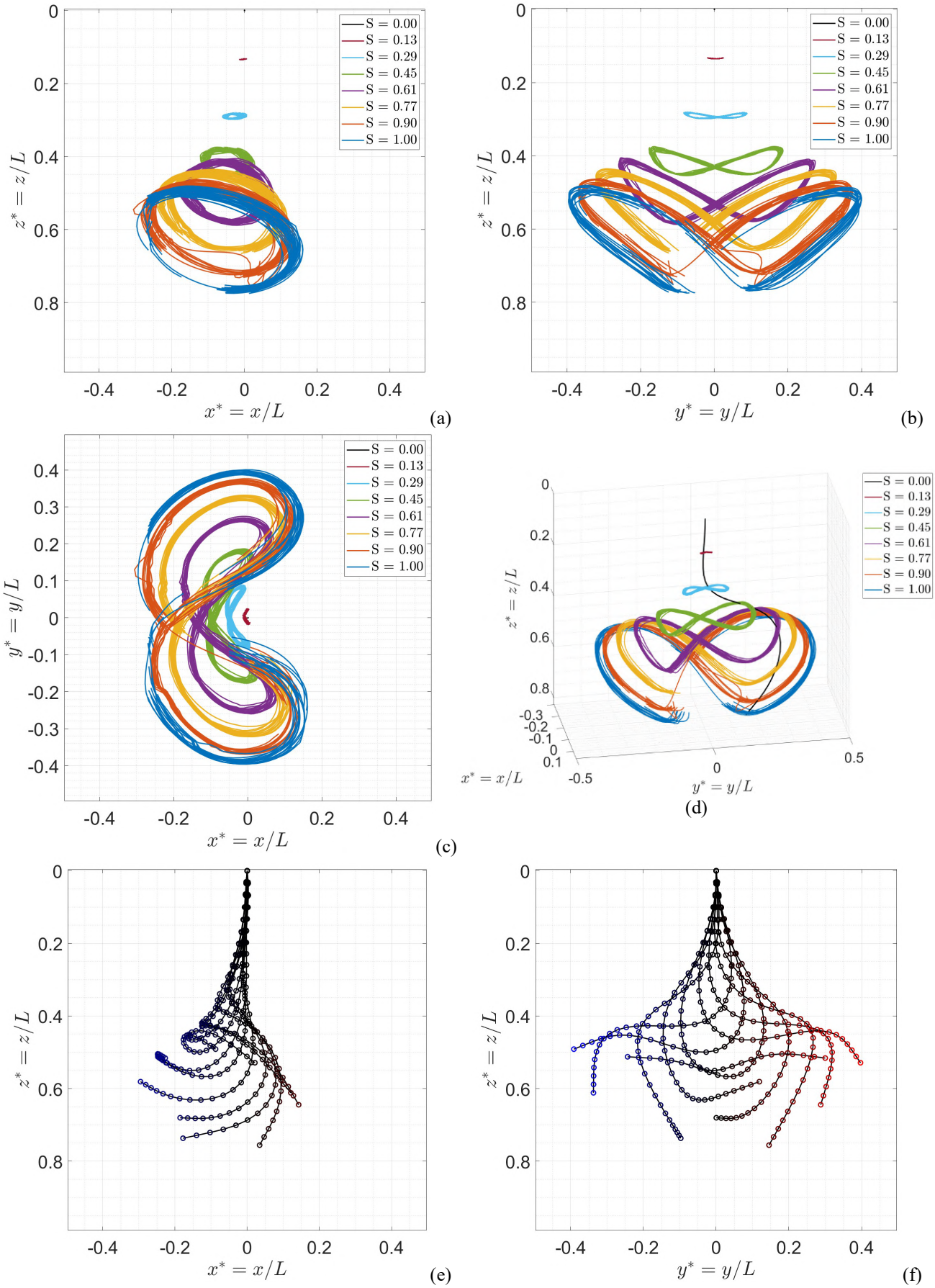

Figure 6: (a), (b) and (c) Orbits projections onto the *xz*, *yz* and *xy* (horizontal) planes, respectively. (d) Three-dimensional orbits. (e) and (f) Deformed configuration snapshots in *x* and *y* directions, respectively, along vertical axis. Warm colors: positive coordinates; cold colors: negative coordinates. Scales 1:1. Model BH-3.

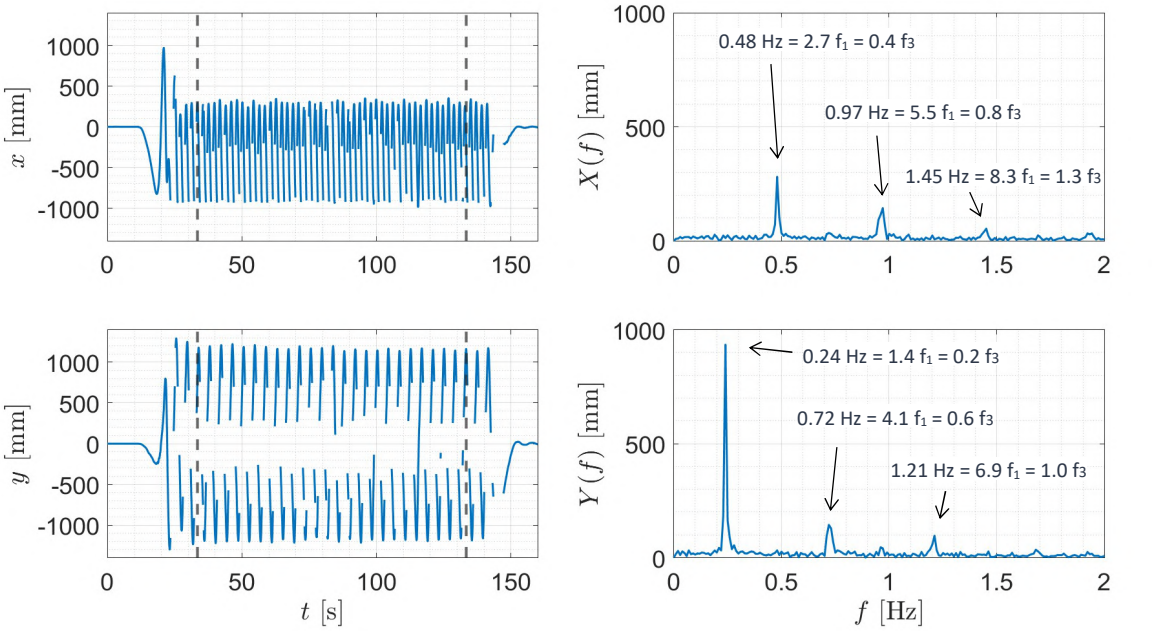

(a)

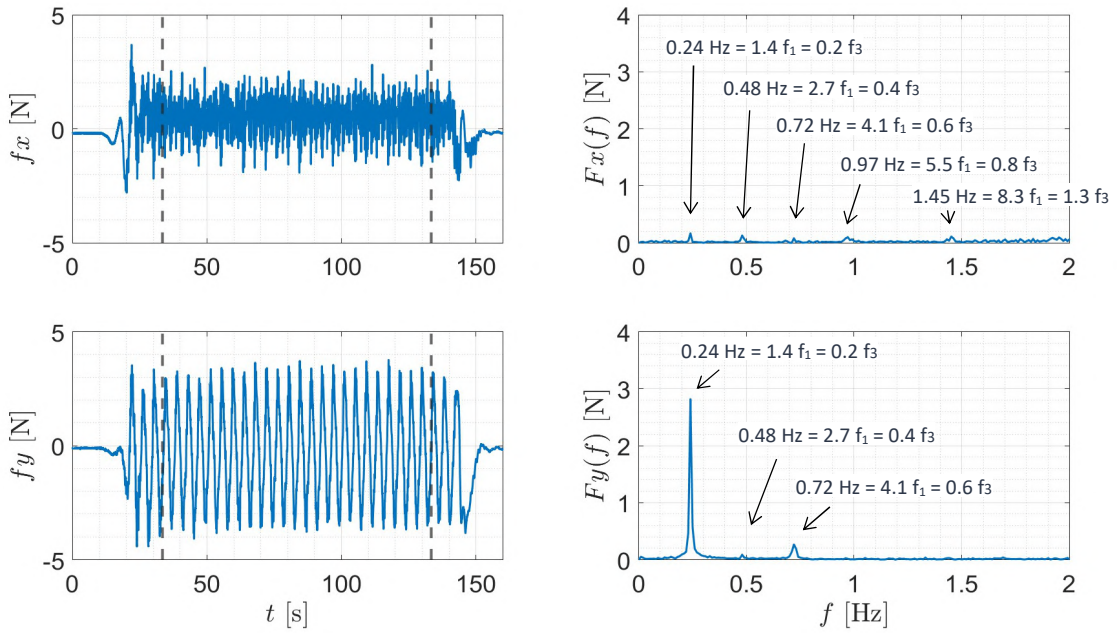

(b)

Figure 7: (a) Tip time series and amplitude spectrum in *x* and *y* directions. (b) Reaction force components at the clamp: time series and amplitude spectrum. Vertical dashed lines indicate the selected part of the signal. Model BH-3.

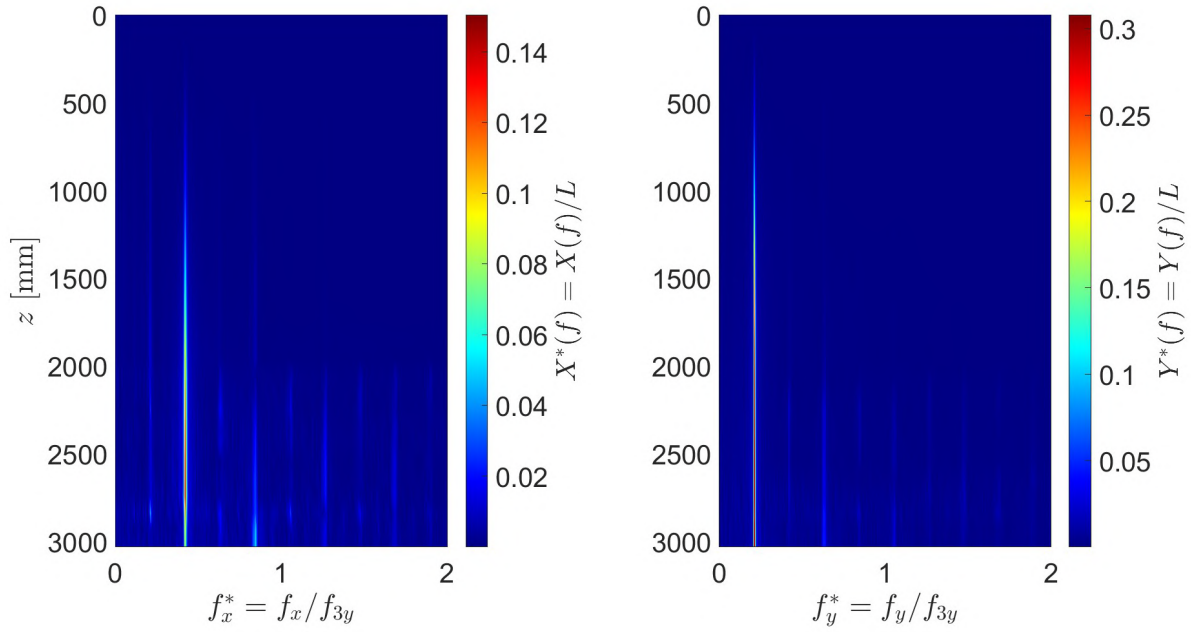

(a)

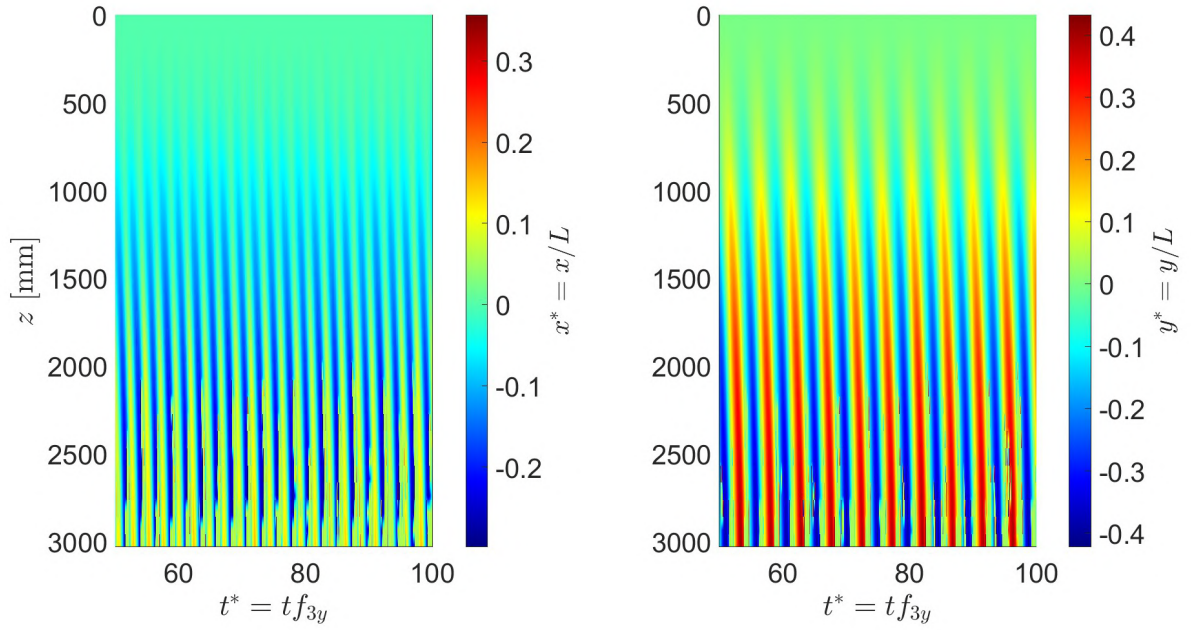

(b)

Figure 8: (a) Amplitude spectra. (b) Amplitude scalograms. Both, along the model's length. *x* (left) and *y* (right) directions. Model BH-3.